$BaTiO_3(001)$-(2×1): Surface Structure and Spin Density

H. L. Meyerheim,[1,*] A. Ernst,[1] K. Mohseni,[1] I. V. Maznichenko,[2] S. Ostanin,[1] F. Klimenta,[1] N. Jedrecy,[3] W. Feng,[1] I. Mertig,[1,2] R. Felici,[4] and J. Kirschner[1,2]

[1]*Max-Planck-Institut für Mikrostrukturphysik, Weinberg 2, D-06120 Halle, Germany*
[2]*Institut für Physik, Martin-Luther-Universität Halle-Wittenberg, D-06099 Halle, Germany*
[3]*Institut des Nano Sciences de Paris, UPMC-Sorbonne Universités, CNRS-UMR7588, 75005 Paris, France*
[4]*ESRF, B. P. 220, F-38043 Grenoble Cedex, France*

(Received 21 December 2011; published 25 May 2012)

Using surface x-ray diffraction and *ab initio* calculations we present a model of the $BaTiO_3(001)$-(2×1) surface structure, which has not been considered so far. While the crystal is terminated by two TiO_2 layers similarly to $SrTiO_3(001)$-(2×1), we find that one out of two surface layer Ti-atoms resides in a tetragonal pyramidal oxygen environment. This peculiar geometry leads to a metallic and magnetic surface involving local magnetic moments up to $2\mu_B$ in magnitude located at surface Ti and O atoms. Our results are important for the understanding of the intrinsic surface metallicity of insulating oxides in general.

DOI: 10.1103/PhysRevLett.108.215502 PACS numbers: 68.35.B−, 61.05.cp, 68.47.Gh, 71.15.Mb

Perovskite (PV) type oxides play a central role in the field of oxide electronics. For instance, the archetype ferroelectric $BaTiO_3$(BTO) has attracted much interest motivated by applications in multiferroic tunnel junctions [1–3], which might open new functionalities in the field of spintronics [4]. Similarly, heteroepitaxial PV structures such as $SrTiO_3$(STO)/$LaAlO_3$ have become a central topic in solid state physics owing to the presence of a two-dimensional (2D) electron gas at the interface [5]. Quite recently, a 2D electron gas has also been shown to exist at the surface of a vacuum cleaved bulk STO(001) crystal [6], but a detailed relation of the surface metallicity to the geometric structure remained elusive. This shows that despite the abundance of experimental and theoretical work on the physical properties of PV interfaces and surfaces, the knowledge about their atomic geometry is surprisingly scarce.

More than 30 years ago, the first studies of the BTO and STO(001) surfaces have been published [7,8], reporting a (2×1) and a (2×2) reconstruction. More recent investigations identified a number of additional reconstructions for STO(001: $c(6 \times 2)$, $c(4 \times 2)$ [9], $(\sqrt{5} \times \sqrt{5})$ [10], (2×1), $c(4 \times 4)$, $c(4 \times 2)$, and (2×2) [11–15]. Similarly, for BTO(001) a series of reconstructions were also reported [(1×1), (2×1), $c(2 \times 2)$, (2×2), $(\sqrt{5} \times \sqrt{5})$, (3×1), (3×2), and (6×1)] [16–19].

Quantitative determinations of the atomic geometry exist only for the STO(001)-(2×1) and (2×2) reconstructed surface, for which a double layer TiO_2 termination has been found [12,15]. The model was recently supported by theory [19]. By contrast, there is no experimental study concerning the atomic geometry of the BTO(001)-(2×1) reconstruction. By surface x-ray diffraction (SXRD) we provide direct evidence for a structural model, which has not been considered so far. In combination with *ab initio* calculations we show that the atomic structure is directly linked to the metallic character of the surface and to the appearance of large magnetic moments up to $2\mu_B$ located at Ti and O atoms.

The experiments were carried out at the beam line ID03 of the European Synchrotron Radiation Facility (ESRF) using an ultrahigh vacuum (UHV) diffractometer. Polished BTO(001) samples ($\varnothing = 5$ mm, $d = 3$ mm) were purchased from Mateck GmbH (Germany). The (2×1) reconstruction was prepared by mild Ar^+ ion sputtering (1 keV, partial pressure 3×10^{-5} mbar, sample current $I_S \approx 0.6$ μA) for 30 min followed by two annealing cycles of 20 min each at a temperature of about 850–900 °C. Without sputtering only the (1×1) metric was observed.

After this preparation procedure the crystal is black and semiconducting, which is attributed to the formation of bulk oxygen vacancies (see, e.g., Ref. [16]). Low energy electron diffraction showed a two domain (2×1) diffraction pattern with no indications of other reconstructions such as $p(2 \times 2)$, as observed for STO(001) [15]. No contaminants were detected on the basis of Auger electron spectroscopy. Scanning tunnelling microscopy experiments indicated 4 Å high steps in accordance with the presence of only one type of surface termination.

X-ray reflection intensities were collected under grazing incidence ($\alpha_i = 2°$) of the incoming beam ($\lambda = 0.69$ Å). A 2D pixel detector was used allowing the fast and precise collection of SXRD data as described in Ref. [20]. In the first step of the analysis, 16 fractional in-plane reflection intensities [$I(hk\ell)$] with $\ell = 0.2$ reciprocal lattice units (rlu) were collected, reducing to 10 symmetry independent structure factor intensities [$|F(hk\ell)|^2$] after averaging over symmetry equivalent reflections and correcting for instrumental factors. Using SXRD we benefit from the applicability of single scattering theory allowing classical Fourier

analysis of the reflection intensities well known in bulk crystallography [21]. One important condition is fulfilled in the present case, namely, that the fractional superlattice (SL) reflections do not overlap with reflections of other superstructures (as it is the case discussed in Ref. [15]). The direct Fourier inversion of the measured SL intensities yields the z-projected Patterson function [$P(u, v)$] according to: $P(u, v) = \sum |F(hk0)|^2 \cos[2\pi(hu + kv)]$, where the summation runs over all measured reflections and we have set $\ell = 0$ to a good approximation.

Figure 1(a) shows $P(u, v)$, in which solid and dashed lines represent positive and negative contours, respectively. The latter appear because only fractional SL reflections were used for calculation of $P(u, v)$. Maxima correspond to interatomic correlations within the (2×1) superstructure relative to the average (1×1) structure. We emphasize that by selecting the SL reflections, only those parts of the structure which contribute to the (2×1) superstructure are analyzed.

Six symmetry independent peaks labeled by (A) to (F) are identified, which are directly related to the structure model shown in Fig. 1(b) in the projection along [001]. Ti and O atoms are represented as gray and red spheres, respectively. Symmetry independent atoms are labeled as 1–8 (top layer: 1–5, second layer: 6–8). Primed numbers represent symmetry equivalent atoms. The structure model belongs to the class of double layer (DL) TiO_2 structures shown to be energetically favorable by DFT calculations [18,19].

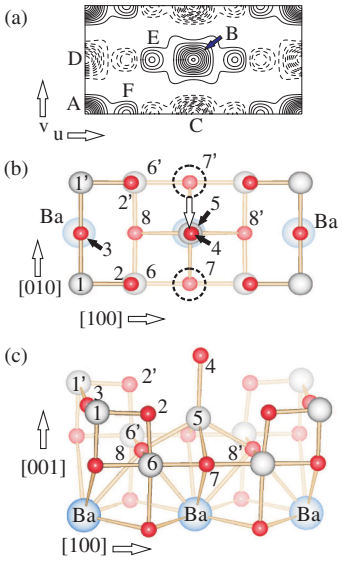

FIG. 1 (color). (a) Patterson function of the projected structure. Solid and dashed contours indicate positive and negative maxima, respectively. Maxima in $P(u, v)$ are labeled by A to F. (b) Structure model of the (2×1) reconstructed unit cell projected along [001]. Atoms within the two top TiO_2 layers are labeled from 1–8. O and Ti atoms are represented by red and gray spheres, respectively. Blue spheres represent Ba atoms as labeled. Dashed circles indicate the positions of Ti atom 5 in the unreconstructed (1×1) structure, which is shifted to the position $(\frac{1}{2}, \frac{1}{2})$ as indicated by the open arrow. (c) Perspective side view of the structure. Interatomic distances in Ångstrom units: 1-2, 1.82; 1-3, 2.01; 2-6, 1.88; 8-6, 2.00; 5-4, 2.30; 5-8, 2.29; 7-6, 2.01; Ba-O (in lane), 2.82; Ba-O (out of plane), 3.09.

The $P(u, v)$ map directly allows to develop a structure model. Peak (A) at the origin corresponds to the self-correlation of all atoms related to the interatomic vector $\vec{R} = \vec{0}$. There are three nontrivial intense peaks, one positive (B) at $(\frac{1}{2}, \frac{1}{2})$ and two negative ones, (C) at $(\frac{1}{2}, 0)$ and (D) at $(0, \frac{1}{2})$. These peaks are consistent with the structure model [Fig. 1(b)] in which the Ti-atom originally located at $(\frac{1}{2}, 0)$ (see dashed circles) is shifted to the position $(\frac{1}{2}, \frac{1}{2})$ in the center of the unit cell. This atom is labeled as 5. An oxygen atom (4) is present on top, as will be discussed below. Thus, peak (B) is (primarily) related to the interatomic vector between Ti-atoms (1) and (5), while peaks (C) and (D) correspond to the interatomic vectors between (1) or (5) and the vacancy at $(0, \frac{1}{2})$, respectively. Furthermore, the less intense positive maxima (E) and (F) can be attributed to atoms, which are shifted out of their bulk truncated (1×1) positions as a result of the rearrangement of the Ti position (see below). Using this starting model, for the fitting of the calculated structure factors to the experimental ones the positions of the atoms 2, 6, and 8 were varied along the [100] direction while preserving the $p2mm$ plane group symmetry. All other positions are fixed by symmetry. In addition, the O atom (4) was placed above the Ti atom (5).

The refinement of the atomic positions yields an unweighted residuum (R_u) of 10% [22]. It should be emphasized that by omitting the O atom 4 only $R_u = 19\%$ is obtained, thus providing an indication for its presence, which also preserves the TiO_2 stoichiometry of the top layer.

Other models led to unsatisfactory fits. For instance, placing the Ti atom (5) above the O atom 8′ at $(\frac{3}{4}, \frac{1}{2})$ and relaxing the symmetry to pm in order to preserve the (2×1) metric, leads to R_u in the 30%–45% range. This model corresponds to the pm-(2×1) structure proposed for STO(001) [12,15].

We went one step further by refining the z positions of the atoms in order to obtain a three-dimensional (3D) structure model using three fractional order SL rods. Including integer order truncation rods into the structure analysis appears not favorable for the present system, since this would require to take into account the complex domain structure of the ferroelectric $BaTiO_3$ bulk with its subtle atomic displacements. Thus, there would be no benefit for the analysis of the (2×1) superstructure whose characteristics are confined to within the top two surface layers. The rods together with the fits (solid lines) are shown in Fig. 2. The table on the right also lists the in-plane structure factor amplitudes normalized to the most intense reflection at $(hk) = (\frac{1}{2}1)$.

The structure model is shown in perspective view in Fig. 1(c). Labeling of the atoms corresponds to that of

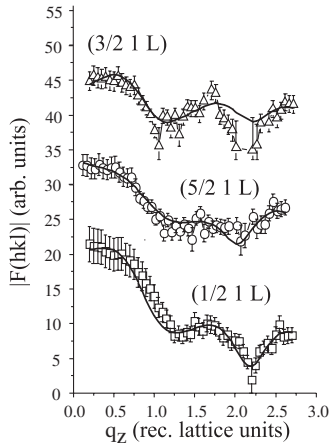

h	k	$\lvert F_{hk0}\rvert$
1/2	0	22± 3
3/2	0	25± 4
5/2	0	25± 4
1/2	1	100± 11
3/2	1	53± 6
5/2	1	63± 7
1/2	2	35± 4
3/2	2	19± 6
1/2	3	56± 6
5/2	3	49± 6

FIG. 2. Measured (symbols) and calculated (lines) structure factor amplitudes for several fractional order rods. Curves are shifted for clarity. The inset lists the normalized in-plane structure factor amplitudes ($|F(hk0)|$) together with their standard deviations.

Fig. 1(b). The Ti atom 5, which is above the third layer Ba atom, is located 0.53 Å below the bulk truncated surface to bind to four O atoms in the second layer (7, 8, and equivalent ones) at a distance of 2.29 ± 0.15 Å. The fifth O atom (4) is located on top at 2.30 ± 0.15 Å. In consequence, Ti atom 5 resides in the center of a tetragonal pyramid.

In contrast to the STO(001)-(2 × 1) reconstruction there is only one instead of two "floating O atoms" per unit cell, which is "loosely bound to the layer beneath" [19]. It is the twofold coordinated O atom 3, whose distance to the two nearest Ti atoms (1, 1′) is equal to 2.01 ± 0.10 Å. Another twofold coordinated but not floating O atom (2) is shifted by 0.17 Å out of its bulk position along the [100] direction as a result of the broken bond to the (now) displaced Ti atom (5). It binds at low distances of 1.82 ± 0.07 and 1.88 ± 0.12 Å to the Ti atoms (1) and (6), respectively. The shifted O atom (2) is directly observable in the P(u, v) map as peak (F), related to its interatomic correlation with the Ti atom (1). Similarly, peak (E) results from a shift (≈ 0.05–0.10 Å) of the second layer oxygen atoms (8, 8') out of their bulk positions to bind to Ti atom (5).

Some interatomic distances are listed in the caption of Fig. 1(c). The z coordinates of the atoms within the second TiO_2 layer were kept identical for simplicity. We find an overall expansion of the spacing between the second TiO_2 layer and the third (bulk like) BaO layer in the range of 5%.

A residual R_u of 11% and a goodness of fit (GOF) [22,23] close to 1 was obtained using all 156 independent reflections. It should be emphasized that the GOF parameter takes into account the ratio between the number of parameters (8) and the number of reflections (156). In the present case owing to the comparatively simple structure and the Fourier filtering process by using SL reflections only, there is a large oversampling (≈ 20) of the fit problem. The collection of SL rods with higher parallel momentum transfer turned out not to be feasible due to their low intensity.

Our experimental results are complemented by *ab initio* calculations. At first, we compared the stability of different possible geometric structures. To this end, we calculated the total energy variation during the structural transition where the Ti atom is displaced out of its bulk position at $(\frac{1}{2}, 0)$ (7) related to the BTO(001)-(1 × 1) structure to the position $(\frac{1}{2}, \frac{1}{2})$ (5) related to the BTO(001)-(2 × 1) superstructure. In a second step, the Ti atom is shifted to $(\frac{3}{4}, \frac{1}{2})$ related to the structure found by Herger *et al.* for STO(001) − (2 × 1) [15]. Simultaneously, the positions of all atoms in the two top surface layers were computed for each lateral displacement of the Ti atom using the VASP code, well known for its precise determination of energetics and forces [24]. The results of our calculations are shown in Fig. 3. All structures differ energetically from each other by only a very small amount (0.1–0.2 eV). Since the surface preparation is a highly nonequilibrium process, all three structures might form. However, as is clear from Fig. 3 the structural transitions require a substantial activation energy: 1.2 eV from BTO(001)-(1 × 1) to BTO(001)-(2 × 1) and 1.6 eV from BTO(001)-(2 × 1) to STO(001)-(2 × 1).

The electronic and magnetic properties were calculated within the density functional theory (DFT) in the local density approximation using a Korringa-Kohn-Rostoker Green-function method, which is specially designed for semi-infinite layered systems. [25]. The most important result is that the BTO(001)-(2 × 1) surface is metallic and magnetic within the DFT calculations independent on the choice of the functional. The VASP code provided similar results.

Figure 4 compares the spin-resolved density of states (DOS) of (a) TiO_2 terminated BTO(001)-(1 × 1) and

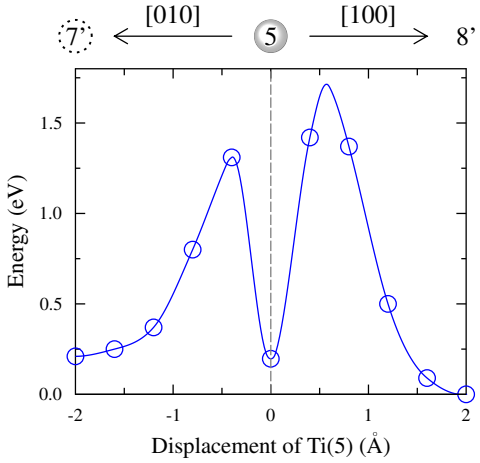

FIG. 3 (color online). Calculated total energy versus Ti-atom displacement. Labels (7′), (5), and (8′) correspond to the Ti position [see Fig. 1(b)] related to the (BTO-(1 × 1), BTO-(2 × 1), and the STO-(2 × 1) structure, respectively (see text).

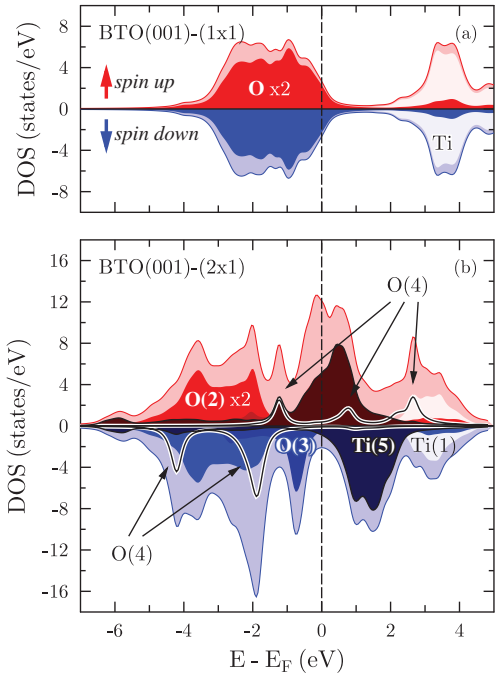

FIG. 4 (color). Calculated spin-resolved density of states for BTO(001)-(1 × 1) (a) and BTO(001)-(2 × 1) (b) atomic labeling corresponds to the structure model in Figs. 1(b) and 1(c) Light colors indicate total spin-resolved DOS.

(b) BTO(001)-(2 × 1). The electronic structure of the (1 × 1) surface was calculated based on the first-principles calculations by Fechner *et al.* [3] indicating that the TiO_2-surface termination is energetically more preferable. In the case of BTO(001)-(2 × 1) the experimental structure parameters of this study were used.

The DOS of BTO(001)-(1 × 1) [Fig. 4(a)] exhibits a quasimetallic behavior which is in agreement with the previous calculations [3]. This kind of metallic character might be destroyed by the presence of impurities and imperfections leading to an insulating surface. The band structure below the Fermi level comprises hybridized Ti 3*d* and O 2*p* states, while bands above the Fermi level in the 3–5 eV range are identified as antibonding Ti 3*d* states. Since the DOS of both Ti and O atoms exhibit an almost identical distribution, a very strong hybridization between Ti 3*d* and O 2*p* states is inferred.

The situation is completely different in the case of BTO(001)-(2 × 1) [Fig. 4(b)], where a strong metallicity is observed. It is mainly a consequence of the hybridization between the Ti atom (5) with the surrounding oxygen atoms involving a shift of the (previously unoccupied) Ti-3*d* states to the Fermi level corresponding to a charge transfer to the Ti atom (5). Simultaneously, we find that, as a result of the low coordination and reduced symmetry, a narrowing of the DOS occurs involving partially unsaturated 2*p* states in the case of the O atoms (3) and (4). In turn this leads to high local magnetic moments.

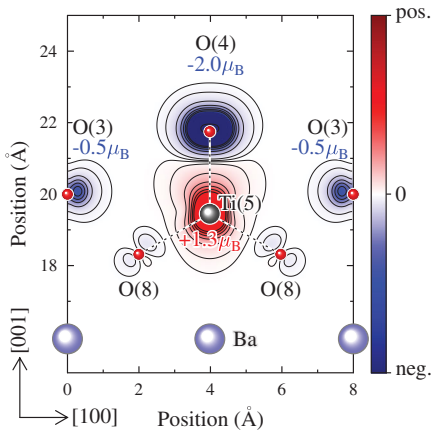

FIG. 5 (color). Spin density and magnetic moments calculated for BTO(001)-(2 × 1).

Figure 5 shows the calculated spin density contour plot in the plane defined by the [100] and the [001] direction. In detail, the atoms Ti (5) and O (4) are antiferromagnetically coupled characterized by magnetic moments of $+1.3\ \mu_B$ and $-2.0\ \mu_B$, respectively. The magnetic interaction in the Ti(5)-O(4) bond is strongly localized. By contrast, O atoms (3) form a magnetic chain along [010] with local magnetic moments of $-0.5\ \mu_B$. The total energy calculations also reveal that the surface is magnetic with the total magnetic moment of $1.5\ \mu_B$.

In summary, our structural analysis of the BTO(001)-(2 × 1) reconstruction has identified an atomic arrangement not considered so far in (001) oriented PV surfaces. The most remarkable unit is a Ti atom in a tetragonal pyramidal environment. This unique structural motif causes symmetry breaking, localization of the electronic states, and charge transfer to the central Ti atom (5) from surrounding oxygen atoms, the latter being directly related to the shift of the otherwise unoccupied 3*d* states to the Fermi level. This leads to the metallization and magnetization which is now identified as an intrinsic property of the surface. We infer that this metallization also contributes to the stabilization of the reconstruction related to the depolarization of the surface. Our model of an intrinsic structurally related strong metallicity might explain the recently reported robustness of the surface metallic character against different doping levels [6], which seems to be a general property of (001) oriented PV surfaces.

We thank F. Weiss for technical support. This work is supported by the DFG through SFB 762.

*hmeyerhm@mpi-halle.mpg.de

[1] E. Y. Tsymbal and H. Kohlstedt, Science **313**, 181 (2006).
[2] C.-G. Duan, S. S. Jaswal, and E. Y. Tsymbal, Phys. Rev. Lett. **97**, 047201 (2006).
[3] M. Fechner, S. Ostanin, and I. Mertig, Phys. Rev. B **77**, 094112 (2008).

[4] S. Valencia *et al.*, Nature Mater. **10**, 753 (2011).
[5] S. Thiel, G. Hammerl, A. Schmehl, C. W. Schneider, and J. Mannhart, Science **313**, 1942 (2006).
[6] A. F. Santander-Syro *et al.*, Nature (London) **469**, 189 (2011).
[7] V. E. Henrich, G. Dresselhaus, and H. J. Zeiger, Phys. Rev. B **17**, 4908 (1978).
[8] R. Courths, Phys. Status Solidi B **100**, 135 (1980).
[9] Q. D. Jiang and J. Zegenhagen, Surf. Sci. **425**, 343 (1999).
[10] T. Kubo and H. Nozoye, Phys. Rev. Lett. **86**, 1801 (2001).
[11] M. R. Castell, Surf. Sci. **505**, 1 (2002).
[12] N. Erdman, K. R. Poeppelmeier, M. Asta, O. Warschkow, D. E. Ellis, and L. D. Marks, Nature (London) **419**, 55 (2002).
[13] K. Johnston, M. R. Castell, A. T. Paxton, and M. W. Finnis, Phys. Rev. B **70**, 085415 (2004).
[14] O. Warschkow, M. Asta, N. Erdman, K. R. Poeppelmeier, D. E. Ellis, and L. D. Marks, Surf. Sci. 573 **573**, 446 (2004).
[15] R. Herger, P. R. Willmott, O. Bunk, C. M. Schlepütz, B. D. Patterson, and B. Delley, Phys. Rev. Lett. **98**, 076102 (2007).
[16] T. Shimizu, H. Bando, Y. Aiura, Y. Haruyama, K. Oka, and Y. Nishihara, Jpn. J. Appl. Phys. **34**, L1305 (1995).
[17] H. Bando, T. Shimitzu, Y. Aiura, Y. Haruyama, K. Oka, and Y. Nishihara, J. Vac. Sci. Technol. B **14**, 1060 (1996).
[18] A. M. Kolpak, D. Li, R. Shao, A. M. Rappe, and D. A. Bonnell, Phys. Rev. Lett. **101**, 036102 (2008).
[19] N. Iles, F. Finocchi, and K. D. Khodja, J. Phys. Condens. Matter Lett. **22**, 305001 (2010).
[20] C. M. Schleptüz, R. Herger, P. R. Willmott, B. D. Patterson, O. Bunk, Ch. Brönnimann, B. Henrich, G. Hülsen, and E. F. Eikenberry, Acta Crystallogr. Sect. A **61**, 418 (2005).
[21] M. J. Buerger, *Kristallographie* (Walter de Gryuter, Berlin, 1977).
[22] The unweighted residual (R_u) is defined as $R_u = \sum ||F^{\text{obs}}| - |F^{\text{calc}}|| / \sum |F^{\text{obs}}|$. GOF is defined by GOF $= [1/(N-P)] \sum [(|F^{\text{obs}}| - |F^{\text{calc}}|)^2/\sigma^2]$. F^{obs}, F^{calc} are the experimental and calculated structure factors, respectively, while N and P represent the number of data points and the number of refined parameters. The standard devation of F_{obs} is given by σ. The summation runs over all data points.
[23] S. C. Abrahams, Acta Crystallogr. Sect. A **25**, 165 (1969).
[24] G. Kresse and J. Furthmüller, Phys. Rev. B **54**, 11 169 (1996).
[25] M. Lüders, A. Ernst, W. M. Temmerman, Z. Szotek, and P. J. Durham, J. Phys. Condens. Matter Lett. **13**, 8587 (2001).